# 論文 / 著書情報
# Article / Book Information

| | |
|---|---|
| Title | Reliability assessment of the physical modeling of liquefaction-induced effects on shallow foundations considering nonuniformity in the centrifuge model |
| Authors | Ritesh Kumar, Kiyonobu Kasama, Akihiro Takahashi |
| Citation | Computers and Geotechnics, Vol. 122, 103558 |
| Pub. date | 2020, 6 |
| DOI | https://doi.org/10.1016/j.compgeo.2020.103558 |
| Creative Commons | See next page. |
| Note | This file is author (final) version. |

# License

**Title**

Reliability assessment of the physical modeling of liquefaction-induced effects on shallow foundations considering nonuniformity in the centrifuge model

**Authors**

Ritesh Kumar; Kiyonobu Kasama; Akihiro Takahashi *

***Corresponding author**

Akihiro Takahashi

Email: takahashi.a.al@m.titech.ac.jp

Tel: +81-(0)3-5734-2593 Fax: +81-(0)3-5734-3577

**Address**

Department of Civil and Environmental Engineering

Tokyo Institute of Technology, Japan

**Computers and Geotechnics, 122, 103558, 2020**

**Original URL:**

**https://dx.doi.org/10.1016/j.compgeo.2020.103558**

**Abstract**

Physical modeling has been widely used to simulate geotechnical earthquake engineering-related problems and to validate finite element numerical models. In both cases, the model ground is usually considered to have uniform soil properties. However, the model ground is prone to spatial nonuniformity and may affect engineering judgment based on physical modeling. This paper presents a reliability assessment of the physical modeling of liquefaction-induced effects on shallow foundations considering the spatial variability in the centrifuge model. Two-dimensional (2D) finite element simulations with the PM4Sand (version 3.1) elastoplastic soil constitutive model are performed for a sufficient number of stochastic realizations. The nonuniformity in the centrifuge model is implemented with stochastic realizations of the overburden and energy-corrected, equivalent clean sand, SPT $(N1)_{60cs}$ values using a spatially correlated Gaussian random field. The reliability of the centrifuge model test is assessed based on the stochastic average settlement and tilt of the foundation-structure system. The implications of the nonuniformity in the centrifuge model on the liquefaction extent of the ground and spectral displacement of the foundation are also investigated.

**Keywords**

Centrifuge model; spatial nonuniformity; stochastic analyses, liquefaction, shallow foundation

## 1. Introduction

Liquefaction has caused severe damage to environments built on shallow foundations, such as settlement, tilting, and sinking, all over the world during many past earthquakes. Numerous instances of bearing capacity failure of shallow foundations due to liquefaction were observed in the 1964 Niigata and 1990 Luzon (Philippines) earthquakes. Most of the damaged buildings were two to four stories built on shallow foundations with relatively thick and uniform deposits of clean sand (Liu and Dobry, 1997; Olarte et al., 2017). Surprisingly, many of the damaged structures were influenced by the liquefaction of thin deposits of silt and silty sand (Bray et al., 2000; Bird and Bommer, 2004) in the 1999 Kocaeli (Turkey) earthquake. Many researchers (Bhattacharya et al., 2011; Tokimatsu and Katsumata, 2012; Yamaguchi et al., 2012) have also elaborated on the role of liquefaction in the severe damage of buildings, specifically in the reclaimed land off the Pacific coast during the 2011Tohoku Earthquake.

Dynamic centrifuge modeling has been widely used to understand the liquefaction–induced effects on shallow foundations resting on presumably uniform deposits of saturated, loose to dense, and clean sand (Yoshimi and Tokimatsu 1977; Liu and Dobry 1997; Dashti et al., 2009; Olarte et al., 2017; Kumar et al., 2019a). Several researchers have used dynamic centrifuge model test results to validate their soil constitutive models and finite element numerical models (Popescu and Prevost, 1993; Byrne et al., 2004; Elgamal et al., 2005; Rayhani and El Naggar, 2008; Montgomery and Boulanger, 2016; Macedo and Bray, 2018).

58 Usually, the predicted behavior of shallow foundations resting on the liquefiable ground using
59 the centrifuge model test and the validation of numerical models are based on the assumption that
60 the model ground has uniform soil properties. However, the centrifuge model ground is prone to
61 spatial nonuniformity even though the model ground is intended to be uniformly reconstituted
62 under gravity conditions (Schofield, 1980; Zhang et al., 2008). The nonuniformity in the centrifuge
63 model is evaluated in model scale. However, units in the prototype scale are used in the presented
64 paper to ensure consistency. Several researchers have attempted to obtain the soil's spatial
65 nonuniformity in the centrifuge model ground. For example, Bolton et al. (1999) used an in-flight
66 cone penetration test at 70g to obtain insight into the model's spatial nonuniformity. They reported
67 that the nonuniformity in the model ground (in terms of tip resistance, void ratio, and normalized
68 cone resistance) might vary with the coefficient of variation (COV) of 2-15% with correlation
69 length as low as 0.2 m in the vertical direction under a controlled environment. The image
70 processing technique was used by White et al. (2003) based on particle image velocimetry (PIV)
71 and close-range photogrammetry. They found the COV of dry density in the range of 1-8%. A high-
72 resolution needle probe technique was adopted by Li et al. (2005) to trace the spatial nonuniformity
73 in the centrifuge model ground. They observed the COV of porosity for loose sand and medium
74 dense sand in the range of 1-4% and 1-6%, respectively. The random field approach (details can be
75 found in Popescu and Prevost, 1995; Zhang et al., 2008) is adopted to estimate the COV and
76 correlation lengths used in this study considering the random sampling error, effects of container

size, and invariability due to method of preparation of the model ground. The estimated COV and the correlation length in the vertical direction are found in the range of 1-6% and 0.5-1.0 m, respectively for the centrifuge experiments at 40g. The estimated correlation length in the horizontal direction is found in the range of 2-6 m. This also reflects the observation of Phoon and Kulhawy (1999) and Phoon and Ching (2014), which suggests that the correlation length in the horizontal direction is often within an order of magnitude (~ 10 times) larger than the correlation length in the vertical direction. Different combinations of COV and correlation lengths are considered to trace the average effects of nonuniformity in the centrifuge model, as recommended by Zhang et al. (2008).

With the increasing use of centrifuge modeling for the performance prediction of shallow foundations and calibration of numerical models, it is essential to understand the reliability of centrifuge model tests. Reliability analyses provide a means of evaluating the combined effects of uncertainties in the parameters involved in the calculations, and they offer a useful supplement to traditional engineering judgment (Duncan, 2000). For a thorough understanding of risk and reliability analyses in geotechnical engineering, readers are suggested to read Christian et al. (1994) and Phoon and Ching (2014). In this paper, an attempt is made to evaluate the reliability of the physical modeling of liquefaction-induced effects on shallow foundations considering the spatial nonuniformity in the centrifuge model. The pouring rate and falling height of Toyoura sand and the pouring direction of the sand hopper are the primary sources of nonuniformity in the centrifuge

model. In addition, the size of the model container is limited and a nonuniform model ground along the container boundaries is inevitable.

Centrifuge model test results are used to validate the numerical modeling scheme, which is carried out using the OpenSees (version 3.0.3) framework (Mazzoni et al., 2006) with the PM4Sand (version 3.1) elastoplastic soil constitutive model (Boulanger and Ziotopoulou, 2017; Chen et al., 2020). Laboratory test results from Chiaro et al. (2012, 2013) are used to calibrate the parameters of the PM4Sand model. The nonuniformity in the centrifuge model is implemented with stochastic realizations of the overburden and energy-corrected, equivalent clean sand, SPT $(N1)_{60cs}$ values using a spatially correlated Gaussian random field (Griffiths and Fenton, 2008; Vanmarcke, 2010; Phoon and Ching, 2014). Two-dimensional finite element simulations are performed for a sufficient number of realizations to account for different combinations of spatial nonuniformity in the centrifuge model, as explained in the subsequent subsections.

## 2. Physical model

A dynamic centrifuge experiment is carried out to investigate the liquefaction-induced effects on shallow foundations resting on a level deposit of liquefiable Toyoura sand. The centrifuge model contains two shallow foundations and associated superstructures, namely, buffer tank (BT) and flare stack (FS), imposing average bearing pressures of 51.2 kPa and 71.2 kPa, respectively, at 0.8 m below the surface of the model ground in the prototype scale, as shown in Fig. 1. Dynamic

centrifuge model test is carried out utilizing the Tokyo Tech Mark III centrifuge facility (Takemura et al., 1999) with a radius of 2.45 m, at a centrifugal acceleration of 40g (N = 40). The centrifuge model test simulates a prototype saturated soil deposit of a depth of 10 m, with a water table located 1.8 m below the top surface. The model ground is prepared using Toyoura sand with a target relative density of 50% by the air pluviation method using a sand hopper with a nozzle outlet. The sand hopper is calibrated in terms of the falling height and pouring rate of the Toyoura sand before preparing the model ground. Multiple transducers (e.g., pore pressure transducers, accelerometers, laser displacement transducers, and potentiometers) are carefully placed at desirable locations during the model ground preparation. More details about the physical modeling of the liquefaction-induced effects on the shallow foundation and the comprehensive interpretation of the centrifuge model test results can be obtained from Kumar et al. (2019b).

## 3. Numerical model

Initially, the numerical tool is validated against the centrifuge model test before performing a series of stochastic analyses to investigate the reliability of the physical modeling of liquefaction-induced effects on shallow foundations considering the spatial nonuniformity in the centrifuge model. Half of the centrifuge model configuration, i.e., the buffer tank and the associated foundation, is considered for the numerical simulations, as shown in Fig. 2. Numerical simulations are carried out with a 2D plane strain solid-fluid fully coupled analysis approach. Rayleigh damping of 1% at a

134 frequency of 1 Hz, corresponding to the first-mode of a typical nonlinear ground response, is used
135 in the analyses.

136 The model ground is modeled using quadrilateral u-p (quadUP) elements (Yang, 2000). The
137 footing is modeled using quadrilateral (quad) elements. The bottom nodes of the model ground are
138 kept fixed in both degrees of freedom. The displacement time series of the Tokachi-Oki ground
139 motion (NS component of the recorded shaking at the Hachinohe Port in 1968) is imposed on the
140 bottom nodes of the model ground during dynamic analyses using the multiple support excitation
141 technique. The footing elements are connected to the model ground using the equal degrees of
142 freedom (equalDOF) technique in OpenSees. The side nodes of the model ground are connected
143 using equalDOF to ensure laminar behavior during the dynamic analyses. All the nodes above the
144 water table are assigned a pore water pressure of zero. The efficacy of mesh size is ensured before
145 performing the numerical analyses. The maximum size of the element at any depth is calculated to
146 ensure the proper wave propagation with respect to the minimum wavelength corresponding to the
147 small-strain shear wave velocity profile of the ground and the maximum frequency of the input
148 ground motion after filtration (bandpass 0.10 Hz – 15 Hz) and baseline correction. The reduction
149 in shear wave velocity due to soil-softening during liquefaction is accommodated with a factor of
150 safety equal to five. In addition, the numerical results (average settlement and tilt of footing) for
151 50% coarser and finer mesh (by length) do not show the significant change in the results
152 corresponding to the adopted mesh.

153 The PM4Sand soil constitutive model is used to capture the dynamic behavior of the model
154 ground during shaking. PM4Sand is a stress-ratio controlled, critical state compatible, bounding
155 surface plasticity model developed for earthquake engineering applications (Boulanger and
156 Ziotopoulou, 2017). This constitutive model requires the specification of three primary input
157 parameters, all of which are dimensionless: the apparent relative density ($D_R$), which controls the
158 dilatancy and stress-strain response characteristics; the shear modulus coefficient ($G_0$), which
159 controls the small strain shear modulus; and the contraction rate parameter ($h_{po}$), which is used to
160 adjust the contraction rate to achieve the target cyclic resistance ratio. The calibrated values of $G_0$
161 and $h_{po}$ for the deterministic analysis (with uniform ground) with $D_R$ = 50% are 347.2 and 0.03,
162 respectively. A detailed description of the secondary parameters and their default values can be
163 obtained from Boulanger and Ziotopoulou (2017).
164 The parameters of the PM4Sand Model are calibrated to achieve a single-amplitude shear strain
165 of 3% during cyclic undrained simple shear loading with an initial static shear stress ratio of zero
166 on a horizontal plane at a single element level within 14.5 - 15.5 cycles. It is to be noted that the
167 model's parameters are calibrated at a single element level, and the response is accepted at the
168 system level. The primal reason for this is that the soil response change with the density which has
169 to be properly modeled in the stochastic analyses. In addition, the parameters are calibrated to
170 ensure that the model exhibits similar cyclic mobility, a similar accumulation rate of the shear strain,
171 and similar small strain shear modulus at a single element level, as observed in the laboratory tests.

Laboratory test results from Chiaro et al. (2012, 2013) are considered for the dynamic behavior of saturated Toyoura sand with a relative density of 50% at a single element level for the generalized calibration of the PM4sand model's parameters.

Fig 3(a) shows a typical response of the calibrated PM4Sand Model for a cyclic stress ratio (CSR) = 0.178, $D_R$ = 50%, and $\sigma'_{vc}$ = 100 kPa during cyclic undrained simple shear loading with an initial static shear stress ratio of zero on a horizontal plane. The PM4Sand model exhibits the ability of shear strain accumulation commonly referred to as cyclic mobility, which is evident from the stress-strain behavior. The stress path is shown in Fig. 3(b). In the first cycle of loading, the vertical effective stress ratio quickly decreases to 80%. After the vertical effective stress ratio decreases to 40%, large shear strains are triggered (as shown in Fig. 3(a)), and the vertical effective stress ratio decreases to nearly zero within a few cycles. The numerically simulated cyclic response at the single element level is obtained after calibrating the parameters of the PM4Sand model to achieve a similar response as observed in the experiment in terms of the cyclic mobility, initial shear modulus, and accumulation rate of the shear strain. Fig 3(c) shows the CSR curves corresponding to single-amplitude shear strains of 3% with an initial static shear stress ratio of zero. It should be noted that each loading cycle is divided into four quarters. For instance, the 10, 10.25, 10.50, and 10.75 cycles mean that the single-amplitude shear strain of 3% is achieved in the first, second, third, and fourth quarters of the $10^{th}$ cycle, respectively, for a corresponding CSR. It is evident from Fig. 3(c) that the PM4Sand model can map the CSR behavior of Toyoura sand as

obtained in the experiment with good agreement.

The ability of the numerical model is examined through the simulation of the liquefaction-induced effects on a shallow foundation at the system level. The capabilities of the PM4Sand model for simulating the dynamic behavior of saturated liquefiable ground at the single element level have been validated using Fig. 3. Time histories of the measured pore pressure, acceleration, and displacement at several locations (as shown in Fig. 2) are compared with the respective numerically simulated time histories. Fig 4 shows the measured and simulated time histories of the excess pore pressure. It is evident that the PM4Sand model can map the overall trend of the excess pore pressure evolution at all locations except that the model exhibits a relatively slower rate of generation of the excess pore pressure in the early phase of shaking. Moreover, the PM4Sand model is also able to capture the maximum magnitude of the excess pore pressure with good agreement.

Fig 5 shows the measured and simulated acceleration time histories along with the computed spectral acceleration ratio. The PM4Sand model shows the marginal attenuation in the acceleration time history at A3 in comparison with the trend observed in the centrifuge model test in the early phase of shaking (before 20 s). The seismic performance of the foundation-structure system on the liquefiable ground significantly depends on the low-frequency component of input shaking. The attenuation or amplification of input wave primarily governed by the liquefaction extent of the ground which is influenced by the nonuniformity in the centrifuge model. Although the numerical model shows the somewhat larger spectral acceleration ratio for the high-frequency content, the

Fourier amplitude of the input shaking in that frequency range is small from the beginning and the difference in the acceleration ratio for the high-frequency range has less impact on the settlement behavior of the structure for liquefaction-related problems. The spiky behavior in the later stage of shaking is caused by the soil dilation and re-stiffening mechanism of the stress-strain curve for the PM4Sand model.

The simulated and measured displacement time histories of the footing are compared in Fig. 6. The simulated rate of the vertical displacement of the footing before 40 s is relatively large in comparison with the measured rate in the centrifuge model test. The settlement progression after shaking is evident for the case of the measured footing settlement, whereas the numerical model does not show such a tendency. The shear-induced settlement and the settlement caused by reconsolidation strains due to simultaneous partial drainage govern the overall evolution of the footing settlement and tilt measured in the centrifuge model test. However, the numerical model seems to overestimate the shear-induced settlement and significantly underestimate the settlement caused by reconsolidation. Several researchers have made similar observations, e.g., Taibet et al. (2007), Dashti and Bray (2013), and Karimi and Dashti (2015, 2016). The numerical models typically exhibit limitations in capturing the settlement caused by partial drainage and reconsolidation during and after shaking because of the characteristics of their constitutive formulations, as reported by Shahir et al. (2012), Boulanger and Ziotopoulou (2017), Karimi and Dashti (2016), and Adamidis and Madabhushi (2019). Overall, it can be said that the simulated

displacement time histories are comparable to the measured ones. In addition, the numerical model can capture the total settlement and the tilt of the footing at the end of the shaking, which is further used for the stochastic investigation, as discussed in subsequent sections.

## 4. Stochastic model

The nonuniform relative density within the centrifuge model ground is mapped using the overburden and energy-corrected, equivalent clean sand, SPT $(N1)_{60cs}$ values as suggested by Montgomery and Boulanger (2016). A series of two-dimensional stochastic dynamic analyses are performed considering the centrifuge model ground properties based on anisotropic, spatially correlated Gaussian random fields of $(N1)_{60cs}$ values. A Gaussian correlation function is used, and the random field is generated through LU decomposition of the covariance matrix as per Constantine and Wang (2012). The PM4Sand model has three primary input parameters ($D_R$, $G_0$, $h_{po}$), which can be calibrated (along with the secondary input parameters) per the randomly generated $(N1)_{60cs}$ values. For a given $(N1)_{60cs}$ value, the relative density ($D_R$) and parameter $G_0$ are computed as follows:

$$D_R = \sqrt{\frac{(N1)_{60cs}}{46}} \quad (1)$$

$$G_0 = \left(\frac{G_{max}}{P_A}\right)\left(\frac{P_A}{P'}\right)^{0.5} \quad (2)$$

where $P'$= the mean effective stress and $P_A$= the atmospheric pressure. The value of $G_{max}$ is computed using the correlation proposed by Andrus and Stokoe (2000) for a soil shear wave

velocity ($V_s$) with a slight modification (Montgomery and Boulanger, 2016) as follows:

$$G_{max} = \rho(V_s)^2 \quad (3)$$

$$V_s = 85[(N1)_{60cs} + 2.5]^{0.25}\left(\frac{P'}{P_A}\right)^{0.25} \quad (4)$$

where $\rho$ is the mass density of the ground, which is assigned a uniform value of 1.92 ton/m$^3$ in the present study. The whole model ground is assigned a uniform permeability value of 0.0002 m/s. More index properties of Toyoura sand can be obtained from Kumar et al. (2019b). The last primary input parameter ($h_{po}$) is calibrated to achieve a single-amplitude shear strain of 3% during cyclic undrained simple shear loading with an initial static shear stress ratio of zero on a horizontal plane at the single element level. The random field of $(N1)_{60cs}$ values with calibrated parameters of the PM4Sand model are implemented into the OpenSees numerical model with the help of MATLAB code. Eighteen different cases of nonuniformity in the centrifuge model are considered as tabulated in Table 1, and a total of forty realizations are generated for each of the cases. The number of realizations is determined based on the convergence of the mean and standard deviation of the average footing settlement and tilt. All the cases have a mean value of $(N1)_{60cs}$ = 12 ($D_R$ ~ 50%) with different combinations of nonuniformity in the centrifuge model. The tabulated coefficient of variation (COV) and scale of fluctuation ($\theta_x$ and $\theta_y$) are considered according to Bolton et al. (1999), White et al. (2003), Li et al. (2005), and Zhang et al. (2008) as described in the introduction section.

A typical spatial distribution of $(N1)_{60cs}$ values for COV = 6%, $\theta_x$ = 2 m, and $\theta_y$ = 1 m for mapping the nonuniformity in the centrifuge model is shown in Fig. 7. Fig 7(a) shows the contours

267 of the $(N1)_{60cs}$ values within the model ground for a typical realization. The cumulative probability
268 distributions of all forty realizations are shown in Fig. 7(b). The values of $(N1)_{60cs}$ vary between 10
269 and 14 for all realizations with different probabilities of occurrence. Fig 7(c) shows that the
270 generated spatial distribution of the $(N1)_{60cs}$ values can be fitted with a Gaussian normal
271 distribution with a specified mean ($\mu$) and standard deviation ($\sigma$).

272 Fig 8 shows the typical variation of the mean and standard deviation of the average footing
273 settlement ((LDT1+LDT2)/2) and tilt ((LDT1-LDT2)/W; W = 4.0 m, the width of the footing). The
274 mean and standard deviation become stable within forty realizations, and hence, a reliable statistical
275 interpretation of the stochastic data can be obtained from the series of nonlinear dynamic numerical
276 simulations. It should be noted that the greater the number of realizations, the better the reliability
277 of the statistical interpretation. However, the numerical computational expense should be taken into
278 account when selecting the total number of realizations without compromising the stability of the
279 mean and standard deviation of the primary stochastic outcomes (e.g., the average settlement and
280 tilt of the footing presented in the paper).

281

282 **5. Results and discussion**

283 ***5.1 Average settlement and tilt of the footing***

284 Two–dimensional stochastic analysis results are presented and compared with the deterministic
285 analysis results in the prototype scale. In the case of deterministic analysis, uniform model ground

286 is assumed with $(N1)_{60cs}$ = 12 ($D_R$ ~ 50%). The deterministic analysis is initially validated with a
287 dynamic centrifuge model test, as explained in Section 3. Fig 9 illustrates the stochastic distribution
288 of the average footing settlement for different combinations of nonuniformity in the centrifuge
289 model. The average footing settlement is calculated by taking the average of the readings of LDTs
290 1 and 2 (the location of LDTs are shown in Fig. 2) at the end of the shaking. The mean (μ) and the
291 standard deviation (σ) of the average footing settlement are found in the ranges of 4.90 cm to 5.12
292 cm and 0.294 cm to 0.508 cm, respectively. It is evident that the mean values of stochastic average
293 footing settlement for different combinations of nonuniformity in the centrifuge model (as
294 tabulated in Table 1) are comparable to the deterministic values of the average footing settlement.
295 However, a relatively wide range of standard deviations cannot be ignored, and the implications of
296 the atypical distributions of the average footing settlement (as shown in Fig. 9) are subsequently
297 discussed with the help of Fig. 11.

298 Fig 10 shows the stochastic distribution of the footing tilt for different combinations of
299 nonuniformity in the centrifuge model. The footing tilt is calculated using the readings of LDTs 1
300 and 2 as (LDT1 - LDT2)/4.0 (the width of the footing is 4.0 m, as shown in Fig. 2) at the end of
301 the shaking. The mean (μ) and the standard deviation (σ) of the footing tilt are found in the range
302 of 0.0021-0.0029 rad and 0.0011-0.0023 rad, respectively. It is evident that the mean stochastic
303 footing tilt for different combinations of nonuniformity in the centrifuge model is significantly
304 larger than the deterministic value of the footing tilt. This notable difference (with a maximum

value of 0.0029 – 0.0013 = 0.0016 rad, which is even more than the deterministic value of 0.0013 rad) in the stochastic mean and deterministic value of the footing tilt suggests that the nonuniformity in the centrifuge model has a significant impact on the tilt of the footing. It should be noted that all of the stochastic distributions of the footing tilt with different combinations of centrifuge model nonuniformity are positively skewed from the deterministic value of the footing tilt, as shown in Fig. 10. This emphasizes that the deterministic numerical simulation (with uniform ground properties) substantially underestimates the tilt of the footing. The observations from Figs. 10 and 11 echo the general notion that the deterministic analyses underestimate the settlement and tilt of the footing. However, the probability of their occurrence must be determined, as shown in Fig. 11.

The probability of deviation of the stochastic average footing settlement and tilt from their deterministic values are evaluated and presented in Fig. 11 for different combinations of nonuniformity in the centrifuge model. The deviations of the average footing settlement and tilt are considered on the positive side (more than the deterministic value) and negative side (less than the deterministic value). The maximum deviation of the average footing settlement and footing tilt determined from their deterministic values, along with the associated probability of occurrence, are tabulated in Table 2 for the ease of interpreting Fig. 11. The probability of the average footing settlement being less than the deterministic value is found in the range of 28.06-39.20%. The maximum deviation of the average footing settlement on the negative side is found in the range of

0.47 cm (with a 4.37% probability of occurrence) to 0.90 cm (with a 3.04% probability of occurrence). However, the probability of the average footing settlement being more than the deterministic value is found in the range of 60.80-70.94%. The maximum deviation of the average footing settlement on the positive side is found in the range of 0.90 cm (with a 2.96% probability of occurrence) to 1.51 cm (with a 0.04% probability of occurrence). The probability of the footing tilt being less than the deterministic value is found in the range of 14.84-20.71%. The maximum deviation of the footing tilt in the negative side is found in the range of 0.0016 rad (with a 1.80% probability of occurrence) to 0.0032 rad (with a 2.20% probability of occurrence). However, the probability of the footing tilt being more than the deterministic value is found in the range of 70.30-85.16%. The maximum deviation of the footing tilt in the positive side is found in the range of 0.0043 rad (with a 1.57% probability of occurrence) to 0.0077 rad (with a 0.06% probability of occurrence). These statistics signify that unlike the average footing settlement, the footing tilt is prone to have a significant deviation from the deterministic value with a relatively large probability of occurrence.

### 5.2 *Expected error*

The numerical model (Fig. 2) is an idealized abstraction of the centrifuge model (Fig. 1). Hence, the model uncertainty may affect the reliability of stochastic analyses (Zhang et al., 2009). A non-dimensional (normalized) root-mean-square error is calculated for the average settlement and tilt

of the footing to trace the severity of the error induced due to model uncertainty under the assumption of the random sampling of nonuniformity as reported by Popescu and Prevost (1995). The expected error ($\varepsilon_n$) for random realizations can be calculated as follows:

$$\varepsilon_n = \frac{\sigma_n}{\mu_n \sqrt{n}} \quad (5)$$

where $\sigma_n$ and $\mu_n$ are the standard deviation and mean of the stochastic average settlement and tilt of the footing, respectively, for n realizations.

Fig 12 shows the expected error magnitude in the estimation of the average settlement and tilt of the footing for different combinations of nonuniformity in the centrifuge model. The expected error is compared with the maximum allowable error ($\varepsilon_{max} = 0.35/\sqrt{n} = 0.055$, for n = 40 realizations, Popescu and Prevost, 1995). A scattered trend in expected error magnitude is observed until 15 and 20 realizations for the average settlement and tilt of the footing, respectively. It is evident that the expected error magnitude is significantly large for fewer realizations (n <10). The footing tilt is prone to have a large expected error magnitude in comparison with the average footing settlement. The observed trends of the expected error magnitude are consistent with those reported by Popescu and Prevost (1995) and Popescu et al., 2004. The expected error magnitude decreases with increasing number of realizations, having a notable margin from the maximum allowable error for a total of forty realizations. This also confirms that forty realizations are sufficient for the reliable statistical interpretation of stochastic data, as explained in Section 4.

### *5.3 Displacement response spectra*

The displacement time history of the input motion (Tokachi-Oki) is applied at the base of the numerical model. The frequency and magnitude of the input shaking fluctuate (amplify or attenuate depending upon the soil-structure interaction) as the wave propagates toward the surface of the ground. The response of the superstructure significantly depends on the characteristics of the shaking at the foundation. An attempt is made to understand the stochastic response of the foundation-structure system in terms of the spectral displacement for different combinations of nonuniformity in the centrifuge model. For each realization, the displacement time history of the footing is recorded during shaking. Then, the spectral displacement (horizontal) is calculated for a wide range of fundamental periods (T = 0.0005 ~ 4 s), considering a damping ratio of 5%. A liquefied ground usually filters the high-frequency content of the incident wave while amplifying the magnitude of the low-frequency content. The amplification in the magnitude of the low-frequency content of the incident wave has a significant impact on the spectral displacement of the foundation-structure system.

Fig 13(a) depicts the mean spectral horizontal displacement of the footing against a wide range of fundamental periods along with the mean (μ) +/- standard deviation (σ) trends. It is found that the spectral displacement starts to deviate from its mean value for periods of more than 0.7 s. This emphasizes that the consideration of nonuniformity in the centrifuge model is essential for structures with long fundamental periods. A total of forty realizations are carried out for each case

of nonuniformity in the centrifuge model, as discussed earlier in Section 4. The spectral displacement corresponding to each realization for long periods, T = 2, 3, and 4 s (for the sake of brevity, only three periods are selected) is used to exhibit the stochastic distributions of the spectral displacement as shown in Fig 13(b). The spectral displacement significantly deviates from its mean value with a significant standard deviation. This emphasizes that the consideration of nonuniformity in the centrifuge model is vital to evaluate the seismic behavior of the foundation-structure system.

### *5.4 Liquefaction potential index*

An attempt is made to evaluate the severity of the liquefaction-induced impact on the foundation-structure system in correlation with the average footing settlement and tilt for different combinations of nonuniformity in the centrifuge model. A liquefaction potential index ($I_L$) is calculated per Iwasaki et al. (1982) and Sonmez and Gokceoglu (2005) with a slight modification as follows:

$$I_L = \int_0^Z F(10 - 0.5Z)dz, \; Z \leq 20 \text{ m} \quad (6)$$

where Z is the depth of the ground (= 10 m in this study), and F is defined as the ratio of the area of the liquefied elements and the total area of the elements under the footing at a depth of Z. An element (mesh is shown in Fig. 2) is considered to be liquefied if the excess pore pressure ratio is more than or equal to 0.9. The excess pore pressure ratio ($r_u$) is defined as the ratio of the excess

400 pore pressure to the initial vertical effective stress. In the original liquefaction potential index
401 (Iwasaki et al., 1982), F is the factor of safety against liquefaction defined as FL. Since FL cannot
402 be obtained explicitly from the calculation, it is replaced with the proportion of the liquefied soil
403 in this study.

404 Fig 14(a) shows that the mean and the standard deviation of $I_L$ (for a typical case of
405 nonuniformity in the centrifuge model with COV = 6%, $\theta_x$ = 4 m, and $\theta_y$ = 0.5 m) become stable
406 within forty realizations; hence, a reliable statistical interpretation of the impact of the severity of
407 ground liquefaction on the behavior of the foundation-structure system can be made. Figs 14(b-c)
408 show the stochastic correlation between $I_L$ and the average footing settlement and the tilt. Nearly
409 90% of the $I_L$ values are found in the range of 8-18, corresponding to an average footing settlement
410 in the range of 4.28-5.46 cm with a few (~10%) scattered values in the range of 18-28. However,
411 nearly 87% of the $I_L$ values are found in the range of 8-18, corresponding to a footing tilt in the
412 range of 0.0010-0.0052 rad, with a few (~13%) scattered values in the range of 18-28.

413 Fig 15 shows the overall range of the average settlement and tilt of the footing with a 95%
414 confidence level considering the different combinations of nonuniformity in the centrifuge model.
415 It can be observed that the stochastic mean values of average footing settlement for different
416 combinations of nonuniformity in the centrifuge model are comparable to the deterministic values.
417 However, the 95% confidence range of the footing tilt significantly deviates from its deterministic
418 value. This observation signifies that the deterministic numerical simulation (with uniform ground

419 properties) substantially underestimates the tilt of the footing, and the footing tilt is prone to be
420 severely affected by the nonuniformity in the centrifuge model.
421
422 **6. Conclusions**
423 A reliability assessment of the physical modeling of liquefaction-induced effects on shallow
424 foundations considering nonuniformity in the centrifuge model is carried out using two-
425 dimensional (2D) stochastic numerical analyses. The numerical modeling scheme is validated at
426 the element level and at the system level by simulating the centrifuge model test, which is
427 performed to investigate the liquefaction-induced effects on the shallow foundation. The PM4Sand
428 elastoplastic soil constitutive model is used to simulate the dynamic behavior of the liquefiable
429 model ground. The nonuniformity in the centrifuge model is mapped with the stochastic
430 realizations of the overburden and energy-corrected, equivalent clean sand, SPT $(N1)_{60cs}$ values
431 using a spatially correlated Gaussian random field. The nonuniformity in the centrifuge model is
432 found to influence the engineering judgment made from the centrifuge model test for various types
433 of problems, such as the average footing settlement and tilt, liquefaction severity of the ground,
434 and implications of the ground-foundation-structure interaction. The stochastic average footing
435 settlements with different combinations of centrifuge model nonuniformity are comparable to the
436 deterministic average footing settlement. However, the nonuniformity in the centrifuge model is
437 found to have a significant impact on the tilt of the footing. It is observed that the deterministic

438 numerical simulation (having uniform ground properties) significantly underestimates the tilt of
439 the footing. Stochastic results also indicated that the liquefaction extent in the model ground varies
440 with the centrifuge model's nonuniformity and is correlated with the effects on the foundation-
441 structure system. The stochastic displacement spectra exhibited that the nonuniformity of the
442 centrifuge model ground should be taken into account, especially for long-period structures. The
443 reliability assessment of the centrifuge model test results is essential for better engineering
444 judgment associated with a desired level of confidence. The presented probabilistic correlations
445 between nonuniformity of the centrifuge model and the response of foundation-structure system
446 possess significant practical importance and provides useful information to assess the reliability of
447 the physical model tests by numerical procedure. For a generalized framework to incorporate the
448 reduction in the epistemic uncertainty, it is necessary to further investigate different scenarios of
449 the applied shaking, foundation-structure system, depth of the water table, and ground conditions.
450

451 **Acknowledgments**

452 The first author sincerely acknowledges the support provided by the Monbukagakusho (Ministry
453 of Education, Culture, Sports, Science, and Technology) scholarship for international graduate
454 students. The authors are also indebted to Dr. Gabriele Chiaro, Senior Lecturer, Department of Civil
455 and Natural Resources Engineering, University of Canterbury, New Zealand, for sharing the results
456 of his triaxial experiments.

## References


1. Adamidis, O., Madabhushi, G. S. (2019). Numerical modelling of post-liquefaction reconsolidation. In Online Proceedings: 2nd International Conference on Natural Hazards & Infrastructure (ICONHIC 2019) (p. 963).
2. Andrus, R. D., Stokoe II, K. H. (2000). Liquefaction resistance of soils from shear-wave velocity. Journal of geotechnical and geo-environmental engineering, 126 (11), 1015-1025. *https://doi.org/10.1061/(ASCE)1090-0241(2000)126:11(1015)*
3. Bhattacharya, S., Hyodo, M., Goda, K., Tazoh, T., Taylor, C. A. (2011). Liquefaction of soil in the Tokyo Bay area from the 2011 Tohoku (Japan) earthquake. Soil Dynamics and Earthquake Engineering 31 (11), 1618-1628. *https://doi.org/10.1016/j.soildyn.2011.06.006*
4. Bird, J. F., Bommer, J. J. (2004). Earthquake losses due to ground failure. Engineering geology 75 (2), 147-179. *https://doi.org/10.1016/j.enggeo.2004.05.006*
5. Bolton, M. D., Gui, M. W., Garnier, J., Corte, J. F., Bagge, G., Laue, J., & Renzi, R. (1999). Centrifuge cone penetration tests in sand. Géotechnique, 49 (4), 543-552. *https://doi.org/10.1680/geot.1999.49.4.543*
6. Boulanger, R. W., Ziotopoulou, K. (2017). PM4Sand (Version 3.1): A sand plasticity model for earthquake engineering applications. Center for Geotechnical Modeling Report No. UCD/CGM-17/01, Department of Civil and Environmental Engineering, University of California, Davis, Calif.
7. Bray, J. D., Stewart, J. P., Baturay, M. B., Durgunoglu, T., Onalp, A., Sancio, R. B., Barka, A. (2000). Damage patterns and foundation performance in Adapazari. Earthquake Spectra 16 (1), 163-189. *https://doi.org/10.1193/1.1586152*
8. Byrne, P. M., Park, S. S., Beaty, M., Sharp, M., Gonzalez, L., Abdoun, T. (2004). Numerical modeling of liquefaction and comparison with centrifuge tests. Canadian Geotechnical Journal, 41 (2), 193-211. *https://doi.org/10.1139/t03-088*
9. Chen, L., Ghofrani, A., Arduino, P. (2020). Prediction of LEAP-UCD-2017 centrifuge test results using two advanced plasticity sand models. In Model Tests and Numerical Simulations of Liquefaction and Lateral Spreading (pp. 423-439).
10. Chiaro, G., Kiyota, T., Koseki, J. (2013). Strain localization characteristics of loose saturated Toyoura sand in undrained cyclic torsional shear tests with initial static shear. Soils and Foundations, 53 (1), 23-34. *https://doi.org/10.1016/j.sandf.2012.07.016*
11. Chiaro, G., Koseki, J., Sato, T. (2012). Effects of initial static shear on liquefaction and large deformation properties of loose saturated Toyoura sand in undrained cyclic torsional shear tests. Soils and Foundations, 52 (3), 498-510. *https://doi.org/10.1016/j.sandf.2012.05.008*
12. Christian, J. T., Ladd, C. C., Baecher, G. B. (1994). Reliability applied to slope stability analysis. Journal of Geotechnical Engineering, 120 (12), 2180-2207. *https://doi.org/10.1061/(ASCE)0733-9410(1994)120:12(2180)*
13. Constantine, P. G., Wang, Q. (2012). Random field simulation. < http://www. mathworks.

com/matlabcentral/fileexchange/27613-random-field-simulation>
14. Dashti, S., Bray, J. D. (2013). Numerical simulation of building response on liquefiable sand. Journal of Geotechnical and Geoenvironmental Engineering, 139 (8), 1235-1249. *https://doi.org/10.1061/(ASCE)GT.1943-5606.0000853*
15. Dashti, S., Bray, J. D., Pestana, J. M., Riemer, M., Wilson, D. (2009). Mechanisms of seismically induced settlement of buildings with shallow foundations on liquefiable soil. Journal of geotechnical and geoenvironmental engineering, 136 (1), 151-164. *https://doi.org/10.1061/(ASCE)GT.1943-5606.0000179*
16. Duncan, J. M. (2000). Factors of safety and reliability in geotechnical engineering. Journal of geotechnical and geoenvironmental engineering, 126 (4), 307-316. *https://doi.org/10.1061/(ASCE)1090-0241(2000)126:4(307)*
17. Elgamal, A., Yang, Z., Lai, T., Kutter, B. L., Wilson, D. (2005). Dynamic response of saturated dense sand in laminated centrifuge container. Journal of Geotechnical and Geoenvironmental Engineering, 131 (5), 598-609. *https://doi.org/10.1061/(ASCE)1090-0241(2005)131:5(598)*
18. Griffiths, D. V., Fenton, G. A. (2008). Risk assessment in geotechnical engineering (pp. 381-399). Hoboken, New Jersey: John Wiley & Sons, Inc.
19. Iwasaki, T., Arakawa, T., Tokida, K. I. (1984). Simplified procedures for assessing soil liquefaction during earthquakes. International Journal of Soil Dynamics and Earthquake Engineering, 3 (1), 49-58. *https://doi.org/10.1016/0261-7277(84)90027-5*
20. Karimi, Z., Dashti, S. (2015). Numerical and centrifuge modeling of seismic soil–foundation–structure interaction on liquefiable ground. Journal of Geotechnical and Geoenvironmental Engineering, 142 (1), 04015061. *https://doi.org/10.1061/(ASCE)GT.1943-5606.0001346*
21. Karimi, Z., Dashti, S. (2016). Seismic performance of shallow founded structures on liquefiable ground: validation of numerical simulations using centrifuge experiments. Journal of Geotechnical and Geoenvironmental Engineering, 142 (6), 04016011. *https://doi.org/10.1061/(ASCE)GT.1943-5606.0001479*
22. Kumar, R., Horikoshi, K., Takahashi, A. (2019a). Centrifuge testing to investigate effects of partial saturation on the response of shallow foundation in liquefiable ground under strong sequential ground motions. Soil Dynamics and Earthquake Engineering, 125, 105728. *https://doi.org/10.1016/j.soildyn.2019.105728*
23. Kumar, R., Sawaishi, M., Horikoshi, K., Takahashi, A. (2019b). Centrifuge modeling of hybrid foundation to mitigate the liquefaction-induced effects on shallow foundation resting on the liquefiable ground. Soils and Foundations, 59(6) (in press). *https://doi.org/10.1016/j.sandf.2019.11.002*
24. Li, Z., Kutter, B. L., Wilson, D. W., Sprott, K., Lee, J. S., Santamarina, J. C. (2005). Needle probe application for high-resolution assessment of soil spatial variability in the centrifuge. In Site Characterization and Modeling (pp. 1-15).
25. Liu, L., Dobry, R. (1997). Seismic response of shallow foundation on liquefiable sand. Journal

of geotechnical and geoenvironmental engineering 123 (6), 557-567. *https://doi.org/10.1061/(ASCE)1090-0241(1997)123:6(557)*

26. Macedo, J., Bray, J. D. (2018). Key Trends in Liquefaction-Induced Building Settlement. Journal of Geotechnical and Geoenvironmental Engineering, 144 (11), 04018076. *https://doi.org/10.1061/(ASCE)GT.1943-5606.0001951*
27. Mazzoni, S., McKenna, F., Scott, M. H., Fenves, G. L. (2006). Open system for earthquake engineering simulation user command-language manual.
28. Montgomery, J., Boulanger, R. W. (2016). Effects of spatial variability on liquefaction-induced settlement and lateral spreading. Journal of Geotechnical and Geoenvironmental Engineering, 143 (1), 04016086. *https://doi.org/10.1061/(ASCE)GT.1943-5606.0001584*
29. Olarte, J., Paramasivam, B., Dashti, S., Liel, A., Zannin, J. (2017). Centrifuge modeling of mitigation-soil-foundation-structure interaction on liquefiable ground. Soil Dynamics and Earthquake Engineering, 97, 304-323. *https://doi.org/10.1016/j.soildyn.2017.03.014*
30. Phoon, K. K., Ching, J. (2014). Risk and reliability in geotechnical engineering. CRC Press.
31. Phoon, K. K., Kulhawy, F. H. (1999). Characterization of geotechnical variability. Canadian geotechnical journal, 36 (4), 612-624. *https://doi.org/10.1139/t99-038*
32. Popescu, R., Prevost, J. H. (1993). Centrifuge validation of a numerical model for dynamic soil liquefaction. Soil Dynamics and Earthquake Engineering, 12 (2), 73-90. *https://doi.org/10.1016/0267-7261(93)90047-U*
33. Popescu, R., Prevost, J. H. (1995). Reliability assessment of centrifuge soil test results. Soil Dynamics and Earthquake Engineering, 14 (2), 93-101. *https://doi.org/10.1016/0267-7261(94)00037-H*
34. Popescu, R., Prevost, J. H., Deodatis, G. (2004). 3D effects in seismic liquefaction of stochastically variable soil deposits. In Risk and variability in geotechnical engineering.
35. Rayhani, M. H., El Naggar, M. H. (2008). Numerical modeling of seismic response of rigid foundation on soft soil. International Journal of Geomechanics, 8 (6), 336-346. *https://doi.org/10.1061/(ASCE)1532-3641(2008)8:6(336)*
36. Schofield, A. N. (1980). Cambridge geotechnical centrifuge operations. Geotechnique, 30 (3), 227-268. *https://doi.org/10.1680/geot.1980.30.3.227*
37. Shahir, H., Pak, A., Taiebat, M., Jeremić, B. (2012). Evaluation of variation of permeability in liquefiable soil under earthquake loading. Computers and Geotechnics, 40, 74-88. *https://doi.org/10.1016/j.compgeo.2011.10.003*
38. Sonmez, H., and Gokceoglu, C. (2005). A liquefaction severity index suggested for engineering practice. Environmental Geology, 48 (1), 81-91. *https://doi.org/10.1007/s00254-005-1263-9*
39. Taiebat, M., Shahir, H., Pak, A. (2007). Study of pore pressure variation during liquefaction using two constitutive models for sand. Soil Dynamics and Earthquake Engineering, 27 (1), 60-72. *https://doi.org/10.1016/j.soildyn.2006.03.004*
40. Takemura, J., Kondoh, M., Esaki, T., Kouda, M., Kusakabe, O. (1999). Centrifuge model tests

571 on double propped wall excavation in soft clay. Soils and Foundations,39 (3), 75-87.
572 *https://doi.org/10.3208/sandf.39.3_75*
573 41. Tokimatsu, K., Katsumata, K. (2012). Liquefaction-induced damage to buildings in Urayasu
574 city during the 2011 Tohoku Pacific earthquake. In Proceedings of the International Symposium
575 on Engineering Lessons Learned from the 2011 Great East Japan Earthquake, 665-674.
576 42. Vanmarcke, E. (2010). Random fields: analysis and synthesis. World Scientific.
577 43. White, D. J., Take, W. A., Bolton, M. D. (2003). Soil deformation measurement using particle
578 image velocimetry (PIV) and photogrammetry. Geotechnique, 53 (7), 619-631.
579 *https://doi.org/10.1680/geot.2003.53.7.619*
580 44. Yamaguchi, A., Mori, T., Kazama, M., Yoshida, N. (2012). Liquefaction in Tohoku district
581 during the 2011 off the Pacific Coast of Tohoku Earthquake. Soils and Foundations 52 (5), 811-
582 829. *https://doi.org/10.1016/j.sandf.2012.11.005*
583 45. Yang Z. (2000). Numerical Modeling of Earthquake Site Response Including Dilation and
584 Liquefaction, PhD Thesis, Dept. of Civil Engineering and Engineering Mechanics, Columbia
585 University, NY, New York.
586 46. Yoshimi, Y., Tokimatsu, K. (1977). Settlement of buildings on saturated sand during
587 earthquakes. Soils Found., 17 (1), 23–38. *https://doi.org/10.3208/sandf1972.17.23*
588 47. Zhang, J., Zhang, L. M., Tang, W. H. (2009). Bayesian framework for characterizing
589 geotechnical model uncertainty. Journal of Geotechnical and Geoenvironmental Engineering,
590 135 (7), 932-940. *https://doi.org/10.1061/(ASCE)GT.1943-5606.0000018*
591 48. Zhang, L. L., Zhang, L. M., Tang, W. H. (2008). Similarity of soil variability in centrifuge
592 models. Canadian Geotechnical Journal, 45 (8), 1118-1129. *https://doi.org/10.1139/T08-066*
593

## Tables

Table 1. Different combinations of nonuniformity in the centrifuge model

| Case | Mean (μ), $(N1)_{60cs}$ | COV (%) | $\theta_x$ (m) | $\theta_y$ (m) |
|---|---|---|---|---|
| A | 12 | 2 | 2 | 0.5 |
| B | 12 | 2 | 4 | 0.5 |
| C | 12 | 2 | 6 | 0.5 |
| D | 12 | 2 | 2 | 1 |
| E | 12 | 2 | 4 | 1 |
| F | 12 | 2 | 6 | 1 |
| G | 12 | 4 | 2 | 0.5 |
| H | 12 | 4 | 4 | 0.5 |
| I | 12 | 4 | 6 | 0.5 |
| J | 12 | 4 | 2 | 1 |
| K | 12 | 4 | 4 | 1 |
| L | 12 | 4 | 6 | 1 |
| M | 12 | 6 | 2 | 0.5 |
| N | 12 | 6 | 4 | 0.5 |
| O | 12 | 6 | 6 | 0.5 |
| P | 12 | 6 | 2 | 1 |
| Q | 12 | 6 | 4 | 1 |
| R | 12 | 6 | 6 | 1 |

COV: coefficient of variation, $\theta_x$ and $\theta_y$: correlation length in X and Y direction (see Fig. 2) respectively

598 Table 2. The probability of deviation of the stochastic average footing settlement and tilt from their deterministic values. A few numbers extracted
599 from Fig. 11 are tabulated in this table

| Different combinations of nonuniformity in the centrifuge model[$] | Probability of exceedance of average footing settlement and tilt in negative side (less than the deterministic value) and positive side (more than the deterministic value) | | | | | | | |
|---|---|---|---|---|---|---|---|---|
| | Average footing settlement | | | | Footing tilt | | | |
| | Negative[*] side (cm) | Probability (%) | Positive[**] side (cm) | Probability (%) | Negative[*] side (rad) | Probability (%) | Positive[**] side (rad) | Probability (%) |
| COV = 2%, $\theta_y$ = 0.5 m | -ve | 38.21 | +ve | 61.79 | -ve | 19.54 | +ve | 80.46 |
| $\theta_x$ = 2 m, 4 m, and 6 m | -0.60 | 1.18 | 0.97 | 0.87 | -0.0029 | 0.17 | 0.0063 | 0.05 |
| COV = 4%, $\theta_y$ = 0.5 m | -ve | 34.84 | +ve | 65.16 | -ve | 16.27 | +ve | 83.73 |
| $\theta_x$ = 2 m, 4 m, and 6 m | -0.48 | 5.39 | 1.10 | 0.19 | -0.0016 | 1.80 | 0.0053 | 0.48 |
| COV = 6%, $\theta_y$ = 0.5 m | -ve | 32.40 | +ve | 67.60 | -ve | 20.68 | +ve | 79.32 |
| $\theta_x$ = 2 m, 4 m, and 6 m | -0.47 | 4.37 | 1.51 | 0.04 | -0.0026 | 0.37 | 0.0076 | 0.01 |
| COV = 2%, $\theta_y$ = 1.0 m | -ve | 28.06 | +ve | 70.94 | -ve | 14.84 | +ve | 85.16 |
| $\theta_x$ = 2 m, 4 m, and 6 m | -0.48 | 6.31 | 0.91 | 0.92 | -0.0017 | 1.49 | 0.0050 | 0.01 |
| COV = 4%, $\theta_y$ = 1.0 m | -ve | 39.20 | +ve | 60.80 | -ve | 17.00 | +ve | 83.00 |
| $\theta_x$ = 2 m, 4 m, and 6 m | -0.90 | 3.04 | 0.90 | 2.96 | -0.0026 | 0.37 | 0.0043 | 1.57 |
| COV = 6%, $\theta_y$ = 1.0 m | -ve | 30.26 | +ve | 69.74 | -ve | 20.71 | +ve | 79.30 |
| $\theta_x$ = 2 m, 4 m, and 6 m | -0.74 | 0.77 | 1.27 | 0.44 | -0.0032 | 2.20 | 0.0077 | 0.06 |

600 $ Maximum values among $\theta_x$ = 2 m, 4 m, and 6 m are tabulated in this table, * -ve is less than the deterministic value, ** +ve is more than the deterministic value
601

602 **Figures**

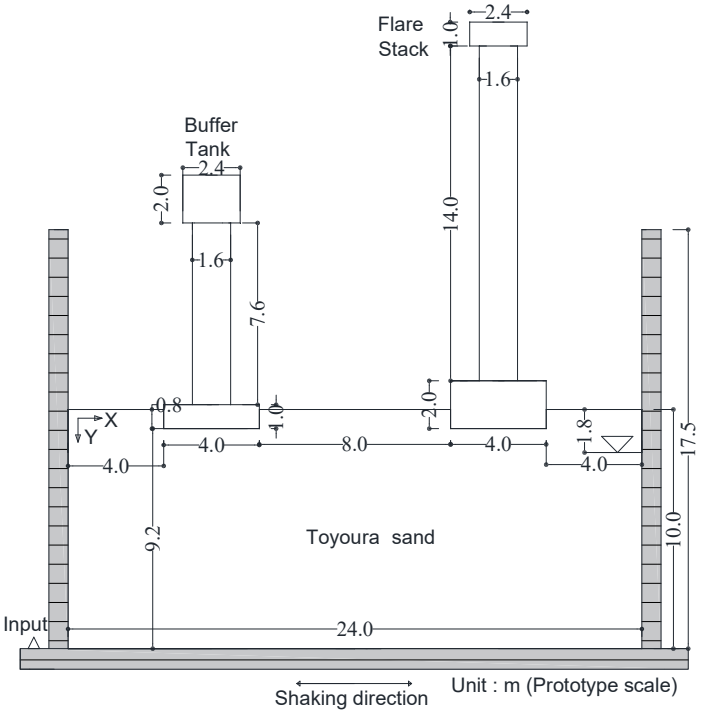


603

604 Fig 1. Centrifuge model configuration in the prototype scale

605

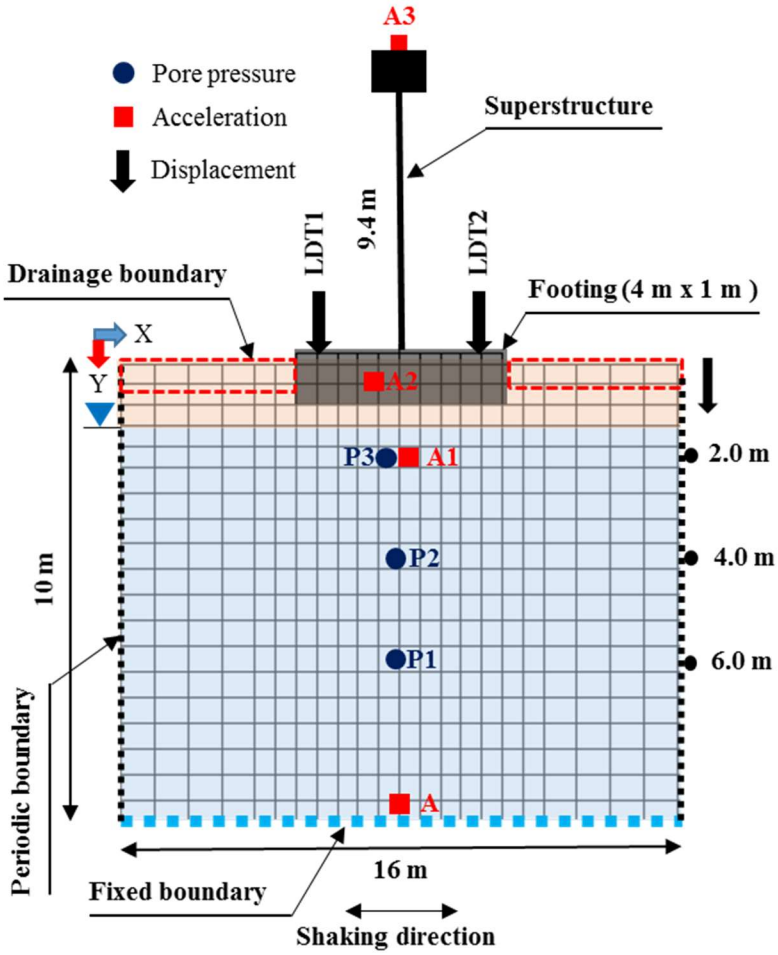


606

607 Fig 2. Two-dimensional (2D) numerical model

608

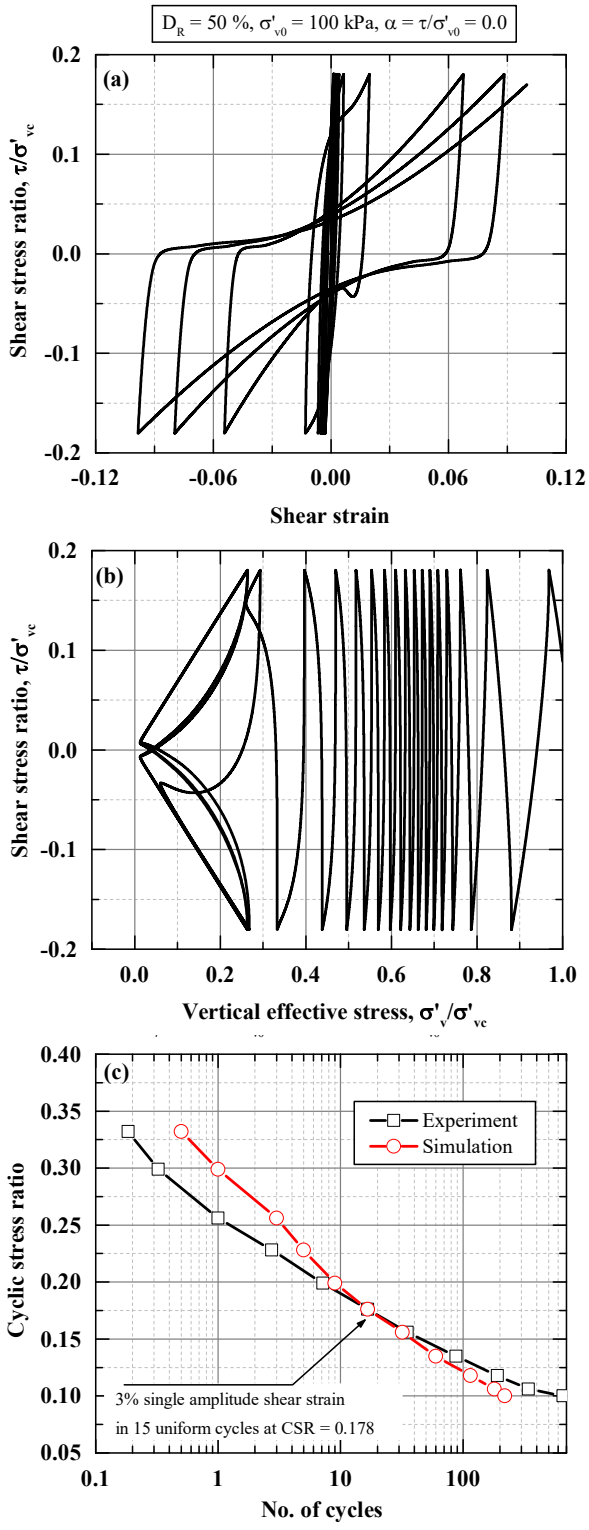


609

610 Fig 3. The response of the calibrated PM4Sand model during cyclic undrained simple shear loading
611 with an initial static shear stress of zero: (a) stress-strain curve, (b) stress path, and (c) liquefaction
612 resistance curves

613

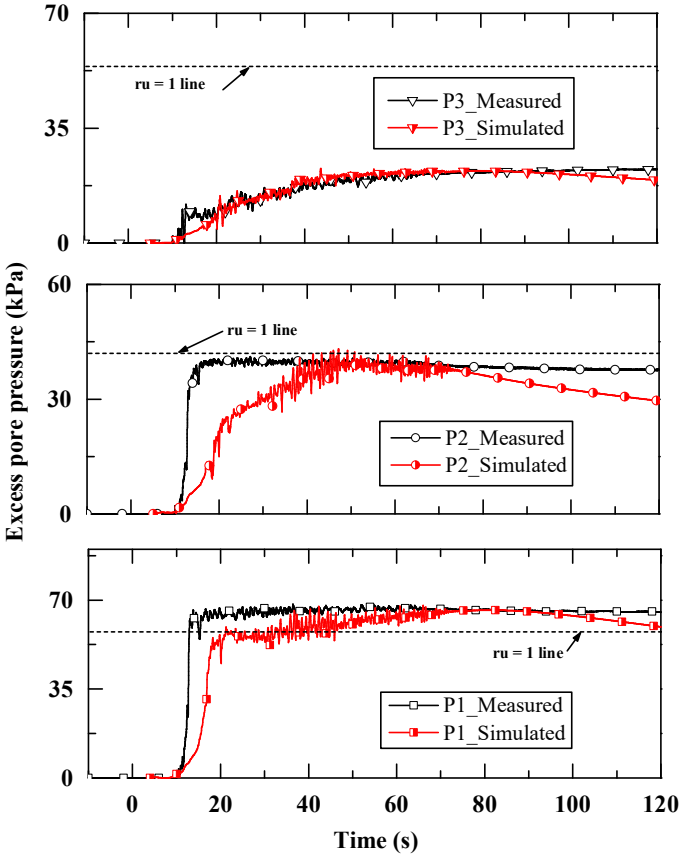


614

615 Fig 4. Measured and simulated excess pore pressure during Tokachi-Oki ground motion

616

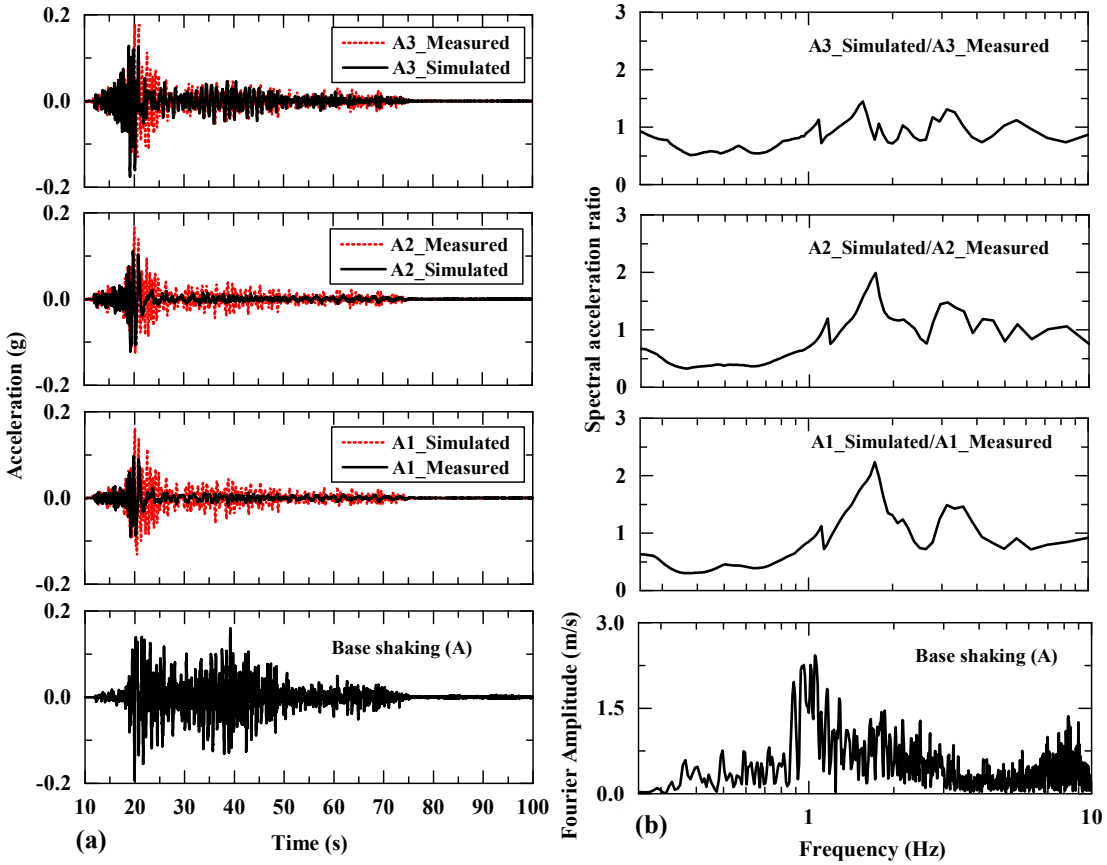


Fig 5. Acceleration response (a) measured and simulated acceleration time histories during Tokachi-Oki ground motion and (b) computed spectral acceleration ratio and Fourier spectrum of applied base shaking

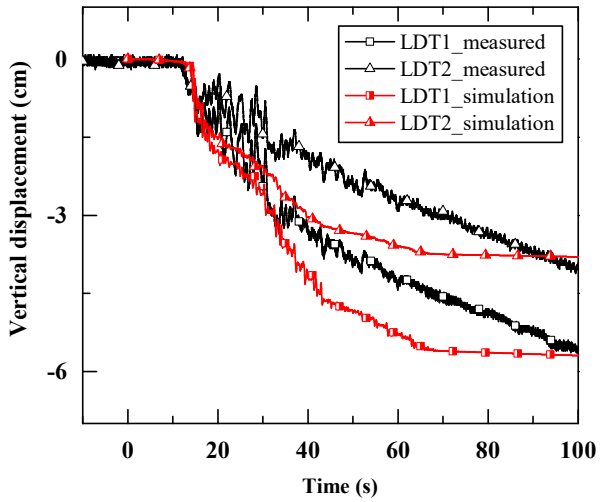


622

623 Fig 6. Measured and simulated footing settlement during Tokachi-Oki ground motion

624

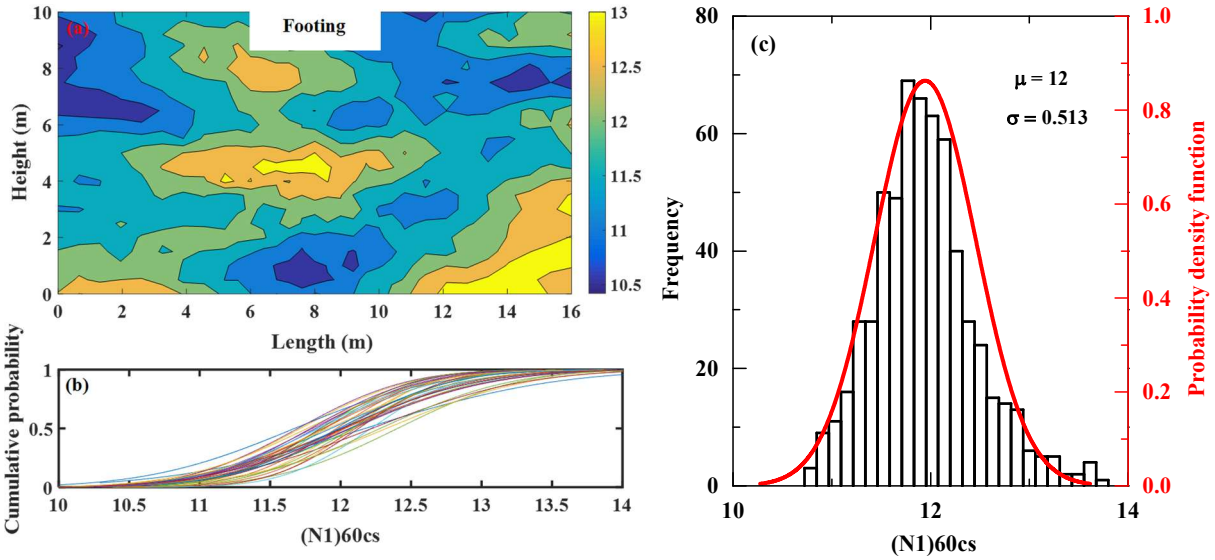


Fig 7. Simulation of nonuniformity in the centrifuge model in terms of the overburden and energy-corrected, equivalent clean sand, SPT $(N1)_{60cs}$: (a) typical random field realization, (b) cumulative probability of forty realizations, and (c) typical stochastic distribution of the generated random field with a fitted probability density function

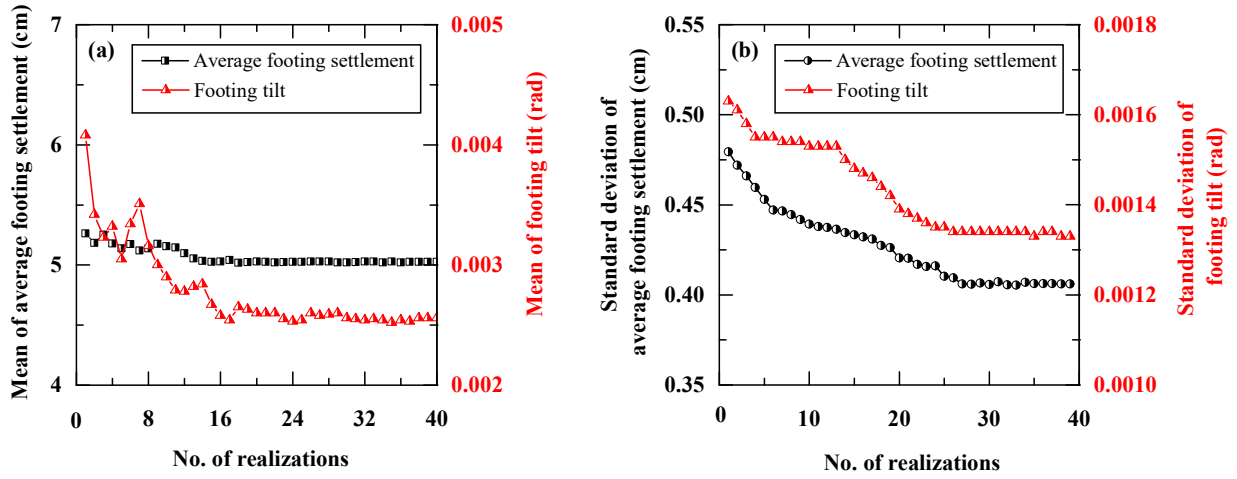


631

632 Fig 8. Typical convergence checks for a total of forty realizations (for COV = 6%, θx = 4 m, and
633 θy = 0.5 m): (a) stability of the mean of the average settlement and tilt of the footing, and (b)
634 stability of the standard deviation of the average settlement and tilt of the footing

635

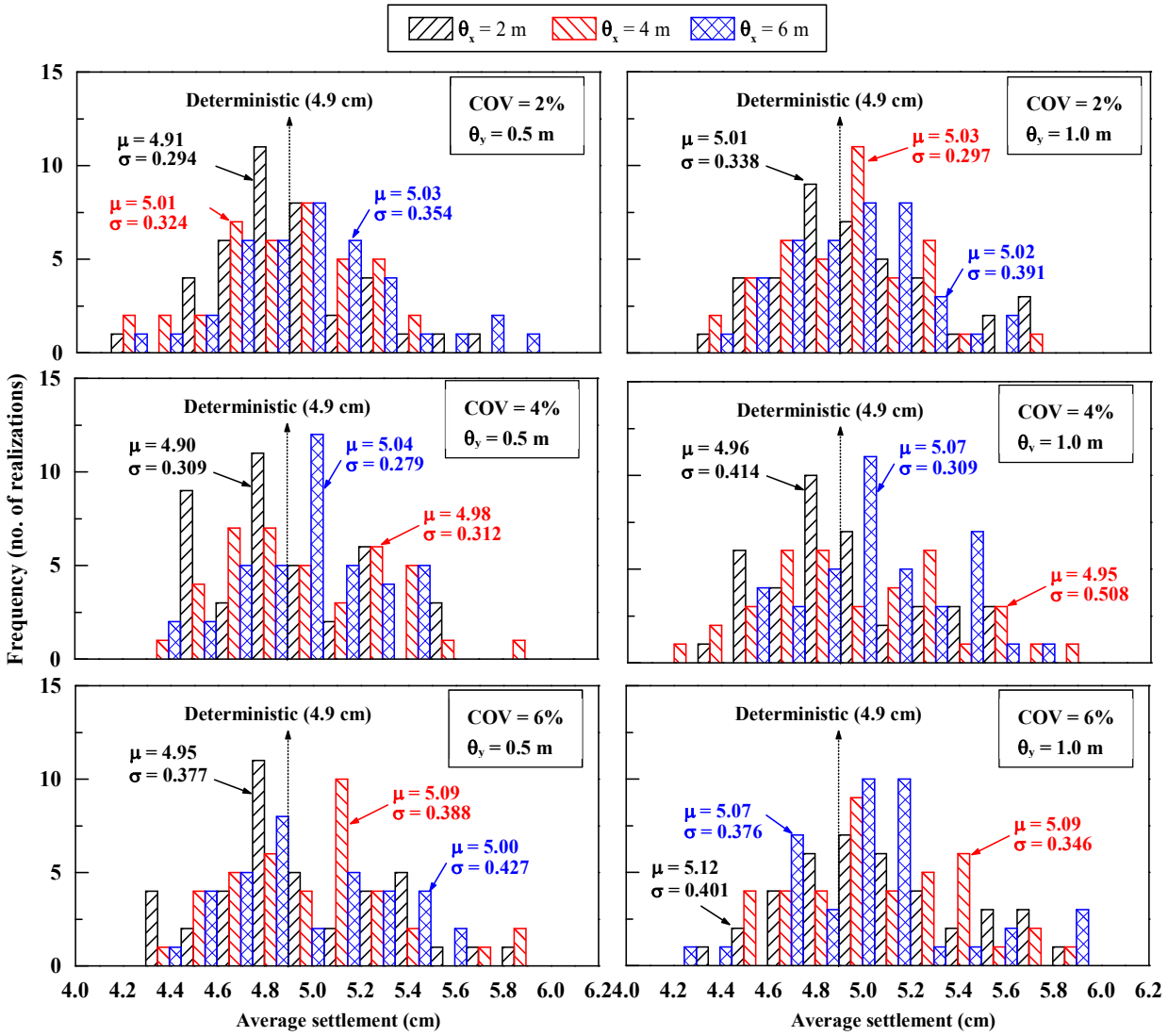


636

637 Fig 9. Stochastic distributions of the average footing settlement for different combinations of
638 nonuniformity in the centrifuge model

639

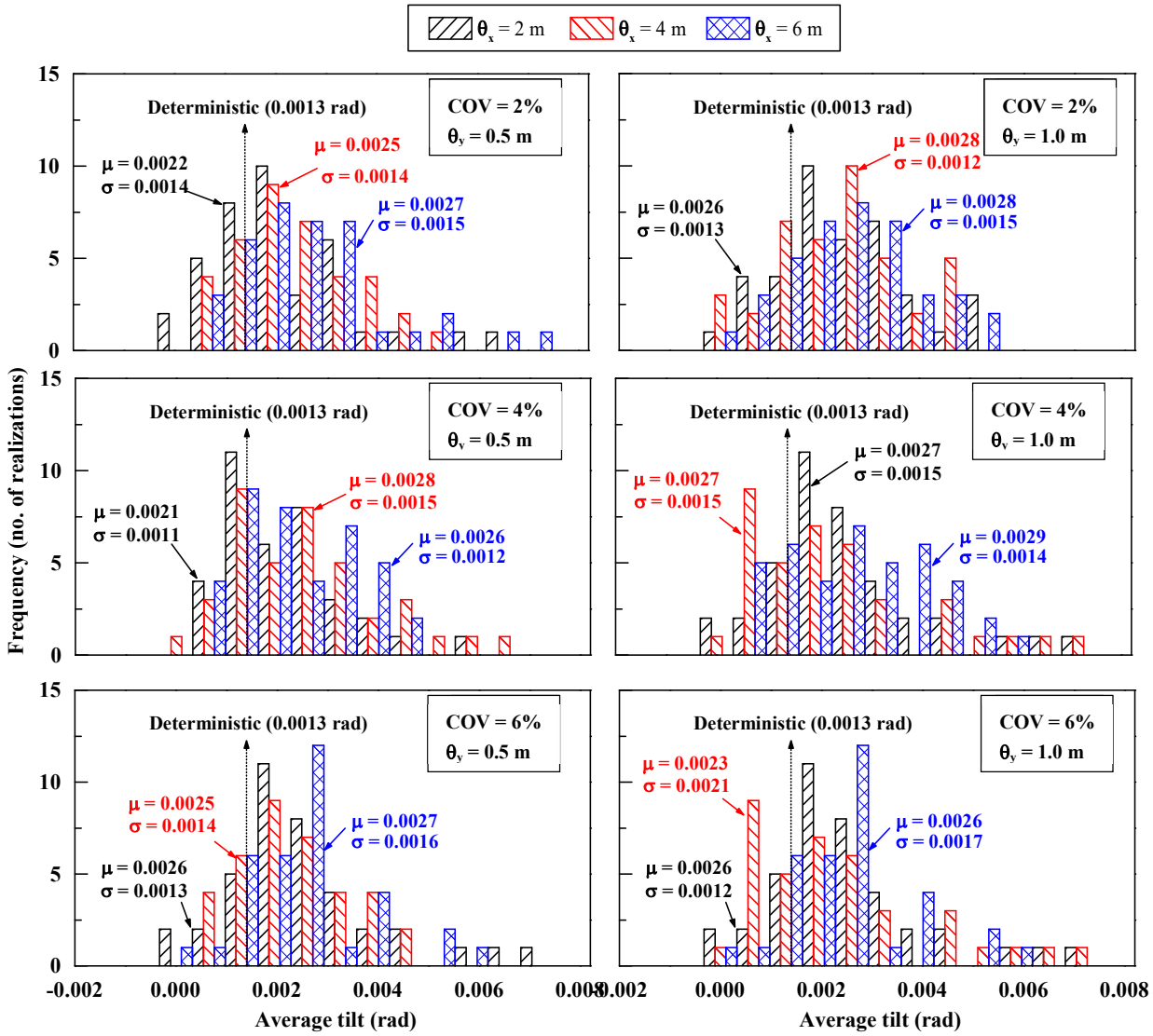


640

641 Fig 10. Stochastic distributions of the footing tilt for different combinations of nonuniformity in
642 the centrifuge model

643

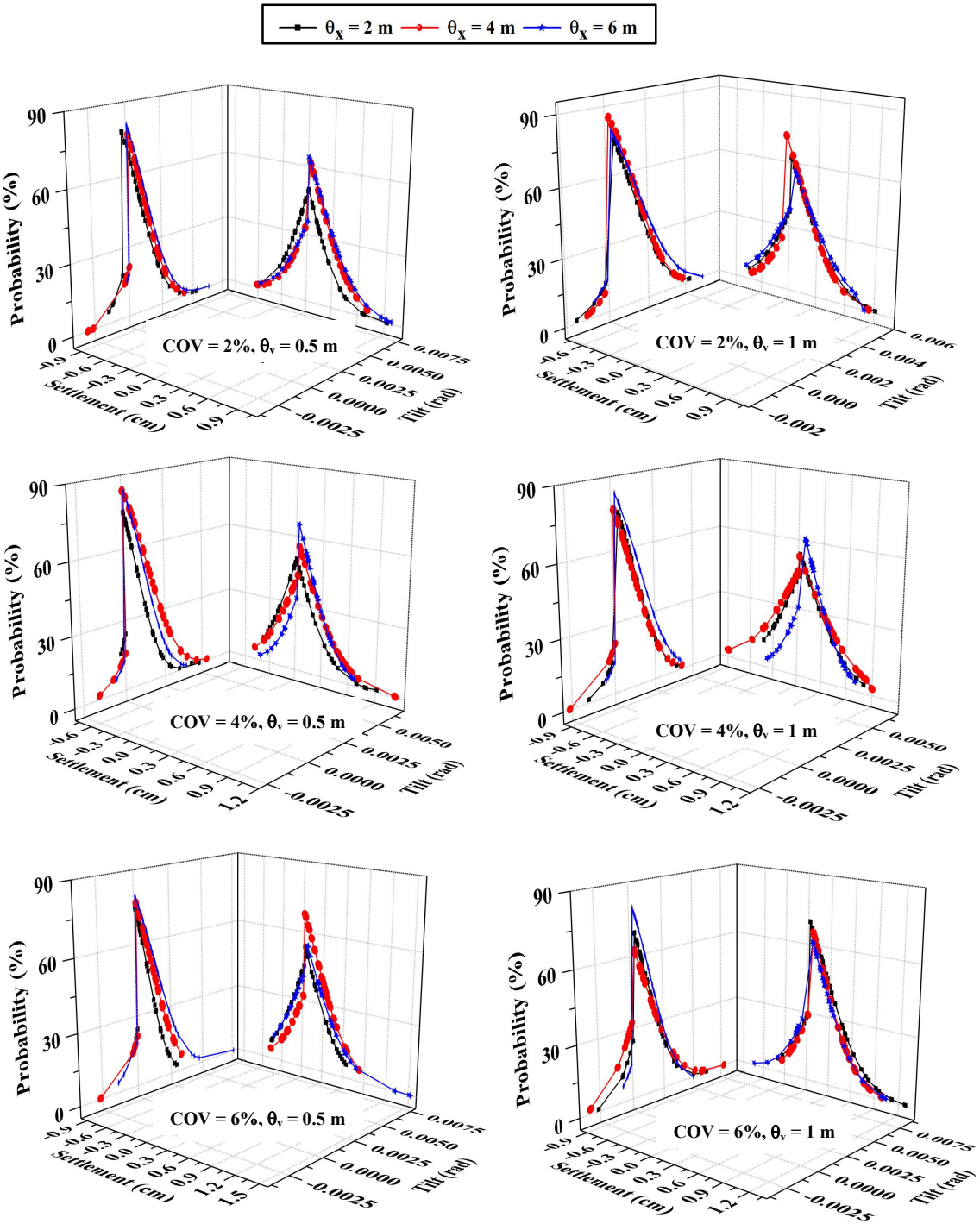


644

645 Fig 11. Probability of the deviation of the average settlement and tilt of the footing from their
646 deterministic values for different combinations of nonuniformity in the centrifuge model (the
647 maximum deviation of the average footing settlement and footing tilt from their deterministic
648 values along with their probability of occurrence are tabulated in Table 2)

649

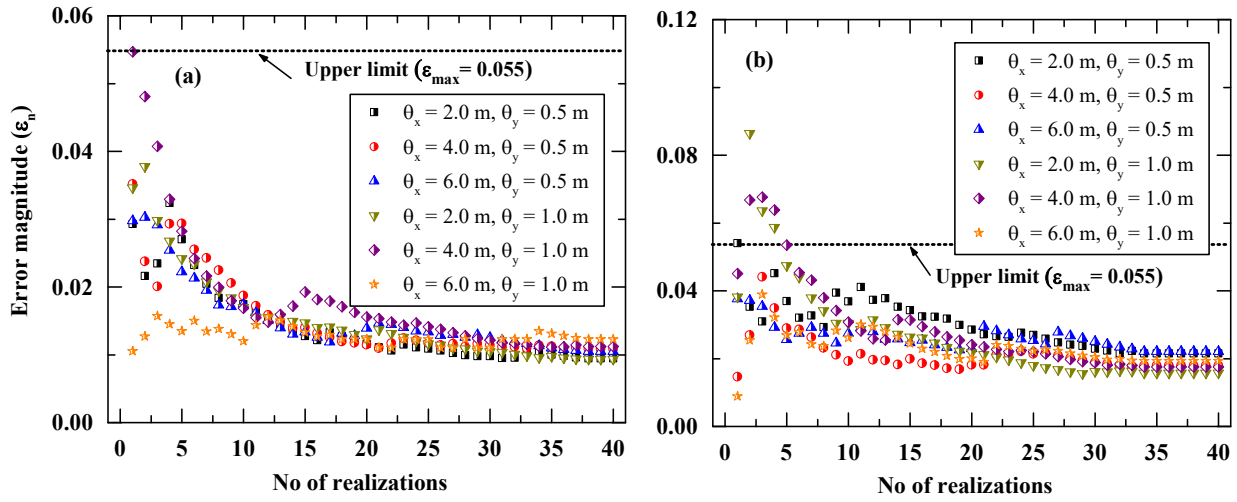


650

651 Fig 12. Expected error magnitude for different combinations of nonuniformity in the centrifuge
652 model (average values for COV = 2%, 4%, and 6%): (a) average footing settlement and (b) footing
653 tilt

654

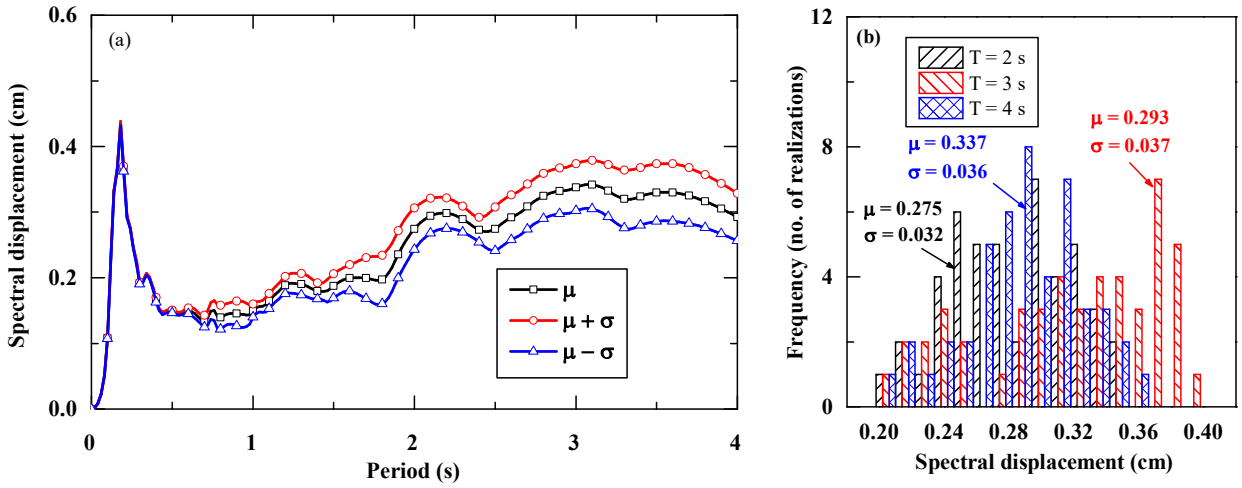


655

656 Fig 13. Response of the foundation-structure system for a typical case of nonuniformity in the
657 centrifuge model (COV = 6%, θx = 4 m, and θy = 0.5 m): (a) spectral displacement with mean (μ)
658 +/- standard deviation (σ) and (b) distributions of the spectral displacement at periods of 2, 3, and
659 4 s

660

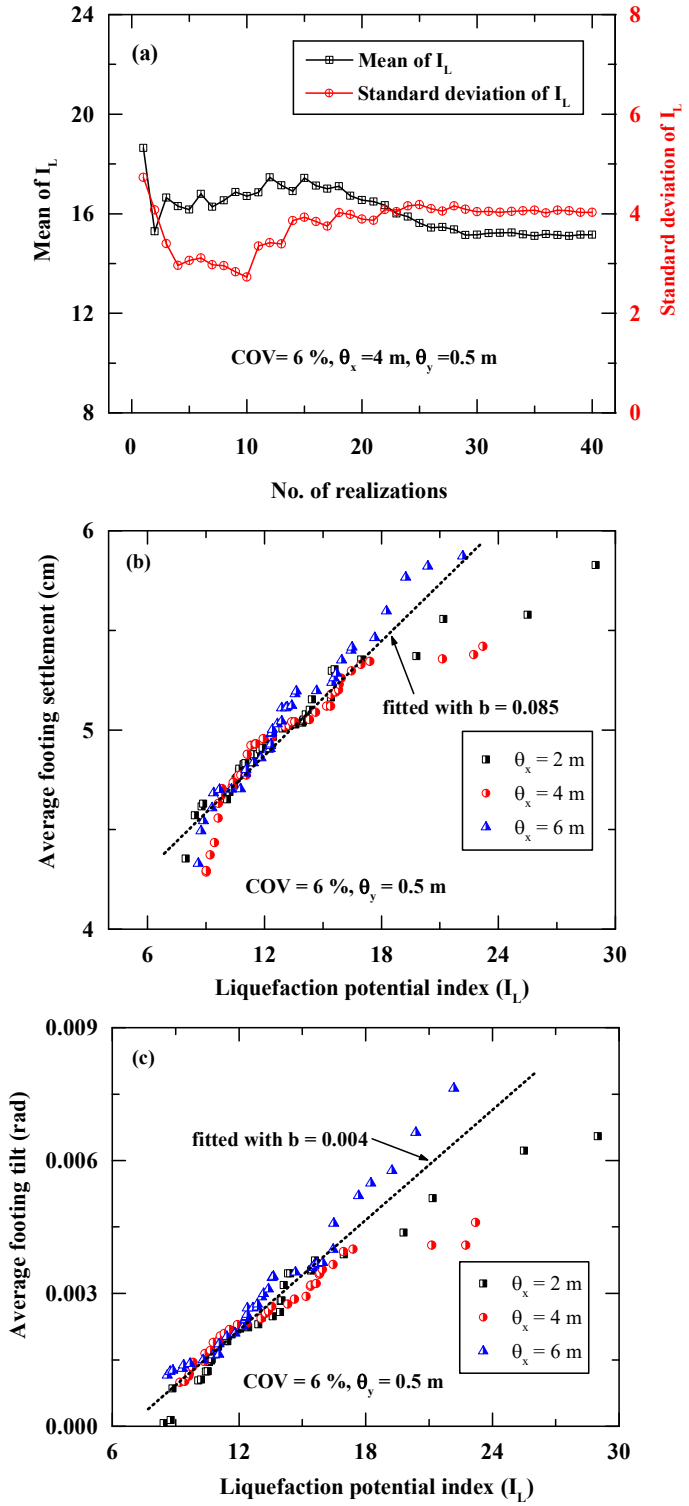


661

662 Fig 14. Liquefaction severity and the response of the foundation-structure system: (a) a typical
663 convergence check for the liquefaction potential index ($I_L$), (b) correlation between the average
664 footing settlement and $I_L$, and (c) correlation between the footing tilt and $I_L$

665

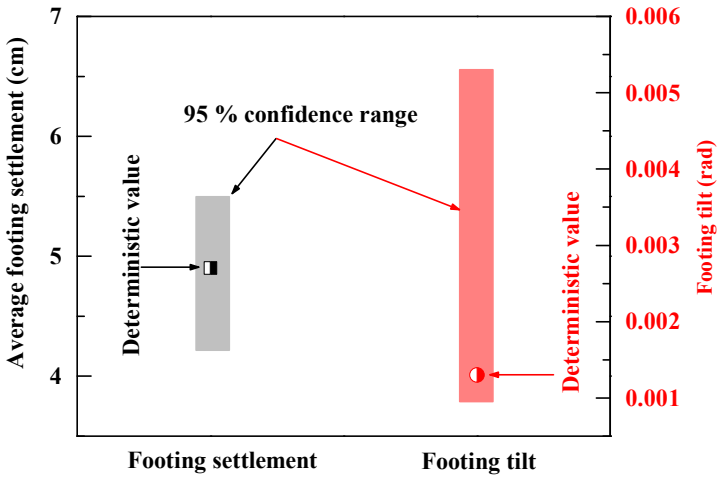


666

667 Fig 15. Stochastic range (with 95% confidence level) of the average settlement and tilt of the
668 footing